

Probing the neutron-skin of unstable nuclei with heavy ion collisions

Junping Yang,¹ Xiang Chen,¹ Ying Cui,^{1,*} Zhuxia Li,¹ and Yingxun Zhang^{1,2,†}

¹*China Institute of Atomic Energy, Beijing 102413, China*

²*Guangxi Key Laboratory of Nuclear Physics and Technology,
Guangxi Normal University, Guilin, 541004, China*

(Dated: April 25, 2023)

To improve the constraints of symmetry energy at subsaturation density, measuring and accumulating more neutron skin data for neutron rich unstable nuclei is naturally required. Aiming to probe the neutron skin of unstable nuclei by using low-intermediate energy heavy ion collisions, we develop a new version of improved quantum molecular dynamics model, in which the neutron skin of the initial nucleus and the mean field potential in nucleon propagation are consistently treated. Our calculations show that the three observables, such as the cross sections of the primary projectile-like residues with $A > 100$ ($\sigma_{A>100}$), the difference of $\sigma_{A>100}$ between $^{132}\text{Sn}+^{124}\text{Sn}$ and $^{124}\text{Sn}+^{124}\text{Sn}$ systems ($\delta\sigma_{A>100}$), and the neutron to proton yield ratio ($R(n/p)$) in the transverse direction, could be used to measure the neutron skin of the unstable nuclei and to constrain the slope of the symmetry energy in the future.

I. INTRODUCTION

The thickness of the neutron skin of a nucleus is characterized as,

$$\Delta r_{np} = \langle r_n^2 \rangle^{1/2} - \langle r_p^2 \rangle^{1/2}, \quad (1)$$

which reflects the difference between the root-mean-square (rms) radii of the neutron and proton density distributions in the nucleus and is strongly correlated with the slope of the density dependence of the symmetry energy[1–6]. Thus, accurate measurements of the neutron skin of a nucleus can be used to constrain the symmetry energy at subsaturation density.

For the determination of the neutron skin of a nucleus, the measurement of the proton and neutron density distributions are needed. The proton density distribution can be accurately determined by electron elastic scattering experiments or isotope shift measurements[7–9], but the neutron density distribution is difficult to measure accurately. The reason is that the neutron is neutral and interacts mainly with hadronic probes. Therefore, the neutron density is mainly probed by proton elastic scattering[10–16], inelastic α scattering[17, 18], coherent pion photoproduction scattering[19], and antiprotonic atoms[20–22], and relativistic energy heavy ion collision (HICs) [23–26]. Another method to measure the neutron density is to use weak electric probes, such as parity violating e-A scattering[27–31] of the Parity Radius Experiment at the Jefferson Laboratory, such as PREX-I [29], PREX-II [30] and CREX [31], or through the coherent elastic neutrino-nucleus scattering[32, 33]. All of the above methods are mainly used to measure the neutron skin for stable nuclei on the nuclear chart.

A great deal of theoretical analysis on the neutron skin of stable nuclei has been performed to constrain the symmetry energy at a subsaturation density [4, 6, 34–42] and

the extrapolated values of the symmetry energy coefficient S_0 and the slope of the symmetry energy L are in 29 – 35 MeV and 5 – 80 MeV[4, 35, 38, 39, 43–57], respectively. However, tension appeared after the PREX-II published the high accuracy ^{208}Pb data since the analysis with a special class of relativistic mean field approach favors a very stiff symmetry energy, i.e., the constrained value of the symmetry energy coefficient $S_0 = 38.1 \pm 4.7$ MeV and the slope of the symmetry energy $L = 106 \pm 37$ MeV [58] are much larger than previously obtained.

To understanding the tension and improving the constraints of the symmetry energy at subsaturation density, two aspects should be investigated. One is to understand the influence of cluster mechanism in the nucleus [59, 60], and we will not touch in this work. Another is to enhance the reliability of constraints by using as many data as possible. The neutron skin data for stable nuclei has been analyzed in Refs. [4, 6, 34–42] to constrain the symmetry energy. For further constraints, accumulating more neutron skin data of neutron-rich unstable nuclei is necessary and it naturally requires to develop a method for measuring the neutron skin of unstable neutron-rich nuclei.

There were some efforts for measuring the neutron skin or the neutron density distribution for unstable nuclei. For example, the total reaction cross sections [61], cross sections of the isovector spin-dipole resonances (SDR) excited by the (^3He , t) charge-exchange reaction [62], the strength of pygmy dipole resonances [63], neutron-removal cross sections in high energy nuclear collisions [64], and charged pion multiplicity ratio (π^-/π^+) ratios in peripheral heavy ion collisions [65, 66], have been used or proposed. Among these methods, the way by using heavy ion collisions is most suitable to measure the neutron skin of a very neutron-rich nucleus since the unstable neutron-rich nuclei in a wide range of isospin asymmetry are mainly produced by the projectile fragmentation mechanism in next generation isotope facility [67].

However, the measurement of the neutron skin of un-

* cuiying@ciae.ac.cn

† zhyx@ciae.ac.cn

stable nuclei via HICs depends on the transport models. In the pioneer transport model calculations [65, 66], the slope of the symmetry energy and the thickness of the neutron skin were treated separately. The separate treatment of the neutron skin in the initial nuclei and the mean field potential in the nucleon propagation increases the theoretical uncertainties for probing the neutron skin of unstable nuclei. Thus, a consistent treatment of the neutron skin in the initialization and the isospin dependent mean field potential in nucleon propagation is highly desired.

In this work, the neutron skin of the initial nucleus is correlated to the mean-field potential more consistently by using the same Skyrme energy density functional in the updated version of improvde quantum molecular dynamics model (ImQMD-L) [68]. Based on the updated ImQMD-L model, the effects of neutron skin on the collision of $^{124,132}\text{Sn}+^{124}\text{Sn}$ at 200 MeV/u are investigated. Our calculations show that the cross sections of primary projectile-like residues with $A > 100$ can be used to distinguish the thickness of the neutron skin. Furthermore, the energy spectra of the yield ratios of emitted neutrons to protons are also analyzed, which can be used for a complementary understanding of the neutron skin effects and the reaction mechanism.

II. THEORETICAL FRAMEWORK

In this part, we briefly introduce the form of the potential energy density in the ImQMD-L model, and how we correlate the neutron skin of an initial nucleus to the mean field potential in nucleon propagation with the same Skyrme energy density functional applied.

A. Potential energy density

In the ImQMD-L model [68], the Skyrme type nucleonic potential energy density without the spin-orbit term is used,

$$u(\mathbf{r})_{sky} = \frac{\alpha}{2} \frac{\rho^2}{\rho_0} + \frac{\beta}{\eta + 1} \frac{\rho^{\eta+1}}{\rho_0^\eta} + \frac{g_{sur}}{2\rho_0} (\nabla\rho)^2 \quad (2)$$

$$+ \frac{g_{sur,iso}}{\rho_0} [\nabla(\rho_n - \rho_p)]^2$$

$$+ A_{sym} \frac{\rho^2}{\rho_0} \delta^2 + B_{sym} \frac{\rho^{\eta+1}}{\rho_0^\eta} \delta^2$$

$$+ u_{md}.$$

Here, ρ is the number density of nucleons which is the summation of neutron density and proton denisity, i.e., $\rho = \rho_n + \rho_p$. δ is the isospin asymmetry which is defined as $\delta = \frac{\rho_n - \rho_p}{\rho_n + \rho_p}$. The α is the parameter related to the two-body term, β and η are related to the three-body term, g_{sur} and $g_{sur,iso}$ are related to the surface terms, A_{sym}

and B_{sym} are the coefficients of the symmetry potential and come from the two- and the three-body interaction terms [69]. u_{md} is the Skyrme-type momentum dependent energy density functional, it is obtained based on its interaction form $\delta(\mathbf{r}_1 - \mathbf{r}_2)(\mathbf{p}_1 - \mathbf{p}_2)^2$ [70], i.e.,

$$u_{md}(\mathbf{r}, \mathbf{p}_i - \mathbf{p}_j) \quad (3)$$

$$= C_0 \sum_{ij} \int d^3p d^3p' f_i(\mathbf{r}, \mathbf{p}) f_j(\mathbf{r}, \mathbf{p}') (\mathbf{p} - \mathbf{p}')^2 +$$

$$D_0 \sum_{ij \in n} \int d^3p d^3p' f_i(\mathbf{r}, \mathbf{p}) f_j(\mathbf{r}, \mathbf{p}') (\mathbf{p} - \mathbf{p}')^2 +$$

$$D_0 \sum_{ij \in p} \int d^3p d^3p' f_i(\mathbf{r}, \mathbf{p}) f_j(\mathbf{r}, \mathbf{p}') (\mathbf{p} - \mathbf{p}')^2.$$

C_0 , D_0 are the parameters related to the momentum dependent interaction. More details about it can be found in Ref. [68].

The parameters in Eq.(2) and (3) are obtained from the standard Skyrme interaction parameters as in Refs.[43, 71]. The connection between the seven parameters α , β , η , A_{sym} , B_{sym} , C_0 , D_0 , used in the ImQMD-L model and the seven nuclear matter parameters, such as, the saturation density ρ_0 , the binding energy at the saturation density E_0 , the incompressibility K_0 , the symmetry energy coefficient S_0 , the slope of the symmetry energy L , the isoscalar effective mass m_s^* , the isovector effective mass m_v^* are given in Ref. [43]. In the following calculations, the g_{sur} and $g_{sur,iso}$ are 24.5 and -4.99 MeVfm², respectively. Thus, one can alternatively use, ρ_0 , E_0 , K_0 , S_0 , L , m_s^* , m_v^* , as input to study the influence of different nuclear matter parameters. In this work, we vary only the L to change the thickness of the neutron skin of the nucleus. All the parameters we used are listed in Table I.

TABLE I. The values of the nuclear matter parameters used in the ImQMD-L. m is the free nucleon mass. m_v^* , m_s^* , m are in MeV, ρ_0 is in fm⁻³, E_0 , K_0 , S_0 , L are in MeV, g_{sur} and $g_{sur,iso}$ are in MeVfm².

K_0	S_0	E_0	ρ_0	m_v^*/m	m_s^*/m	g_{sur}	$g_{sur,iso}$	L
240	30	-16	0.16	0.7	0.8	24.5	-4.99	30,50,70,90,110

B. Initialization with neutron skin

To consistently correlate the neutron skin of initial nuclei with the mean field potential in nucleon propagation, one has to know the neutron and proton density distributions first, and then find a way to approximate the density distributions in the ImQMD-L model.

As discussed in Ref. [68], the Woods-Saxon density profile can be reproduced by sampling the centroids of the wave packets within the hard sphere with a radius that equals to the half density radius of Woods-Saxon

density profile. The relationship of the width of the wave packet σ_r and the diffuseness of the nucleus a is $\sigma_r = f(a) = (1.71217 \pm 0.01548)a + (0.01564 \pm 0.01047)$ fm. Thus, a model that can be used to calculate the Woods-Saxon type density distribution under the same Skyrme energy density functional is needed.

The restricted density variational (RDV) method[72] meets this criteria. In the RDV method, the density distributions

$$\rho_i = \rho_{0i} \frac{1}{1 + \exp(\frac{r-R_i}{a_i})}, i = n, p, \quad (4)$$

are adopted. Where, R_p , a_p , R_n , and a_n are the radius and diffuseness of the proton and neutron density distributions, respectively. ρ_{0i} is the central density of neutrons or protons in the nucleus. These parameters are obtained by minimizing the total energy of the system which is given by,

$$E = \int \mathcal{H} d^3r = \int \left\{ \frac{\hbar^2}{2m} [\tau_n(\mathbf{r}) + \tau_p(\mathbf{r})] + u_{sky} + u_{coul} \right\} d^3r, \quad (5)$$

under the condition of the conservation of the number of particles in the system, i.e., $N = \int \rho_n(\mathbf{r}) d^3\mathbf{r}$ and $Z = \int \rho_p(\mathbf{r}) d^3\mathbf{r}$. u_{coul} is the Coulomb energy density, τ_n and τ_p are the kinetic energy densities of neutrons and protons, respectively. The kinetic energy density in the RDV method is given by the extended Thomas-Fermi (ETF) approach, which includes all terms up to the second order (ETF2) and fourth-order (ETF4) as in Ref. [73]. The same semiclassical expression of the Skyrme energy density functional as in ImQMD-L is used to calculate u_{sky} .

In Table II, we show the RDV results of the binding energy B , the diffuseness parameters a_p and a_n , the half density radius R_p and R_n , the rms radius for neutron and proton, and the thickness of the neutron skin, respectively. Five Skyrme parameter sets, which are represented by the different L values, are used for varying the thickness of neutron skin. Upper part is for ^{124}Sn and bottom part is for ^{132}Sn .

Then, we prepare the initialization as the same as that in Ref. [69], but with different treatments in the following two aspects. The first one is that the centroids of the wave packets for neutron and proton are sampled within the half density radius of the neutron and the proton obtained in the RDV method, i.e., R_n and R_p . Once the positions of all the nucleons have been determined, the density distribution is obtained. Then, the momenta of the nucleons are sampled according to the local density approach. The second one is that the binding energy of the sampled nucleus falling into the range of $B \pm 0.2$ MeV is also required, where B is obtained by the RDV method.

TABLE II. a_p , R_p , a_n , R_n , binding energy B , and rms radius of neutron and proton density distributions for ^{124}Sn and ^{132}Sn obtained with RDV method. L and B in MeV, a_p , R_p , a_n , R_n , $\langle r_p^2 \rangle^{1/2}$, $\langle r_n^2 \rangle^{1/2}$ and Δr_{np} are in fm.

^{124}Sn								
L	B	a_p	R_p	a_n	R_n	$\langle r_p^2 \rangle^{1/2}$	$\langle r_n^2 \rangle^{1/2}$	Δr_{np}
30	-7.971	0.414	5.733	0.514	5.777	4.670	4.865	0.165
50	-8.021	0.415	5.729	0.507	5.811	4.698	4.881	0.183
70	-8.073	0.419	5.707	0.503	5.838	4.687	4.893	0.206
90	-8.129	0.422	5.686	0.496	5.872	4.676	4.907	0.232
110	-8.191	0.426	5.656	0.487	5.909	4.659	4.922	0.263
^{132}Sn								
L	B	a_p	R_p	a_n	R_n	$\langle r_p^2 \rangle^{1/2}$	$\langle r_n^2 \rangle^{1/2}$	Δr_{np}
30	-7.810	0.408	5.827	0.539	5.906	4.762	4.994	0.232
50	-7.889	0.410	5.816	0.532	5.948	4.756	5.013	0.257
70	-7.975	0.413	5.798	0.524	5.990	4.746	5.032	0.286
90	-8.067	0.416	5.771	0.514	6.035	4.730	5.050	0.320
110	-8.166	0.419	5.733	0.502	6.084	4.707	5.068	0.361

III. RESULTS AND DISCUSSIONS

For peripheral collisions at intermediate energy HICs, there are two characteristics associated with the neutron skin of the nuclei. One is the size of the projectile-like and target-like residues, another is the isospin content of the nucleons and light particles which are emitted in the transverse direction. The mechanism of the above two characteristics for peripheral HICs is shown in the schematic diagram in Fig. 1. Panel (a) is the initial stage of the reaction, panel (b) is at the reaction stage, and panel (c) is at the later stage of the reaction where the projectile and target like fragments are formed and the light particles are emitted from the neck region. Thus, one can expect that a larger neutron skin could lead to a larger reaction cross section or larger production cross sections for projectile/target-like residues, more neutrons and neutron-rich light particles emitted.

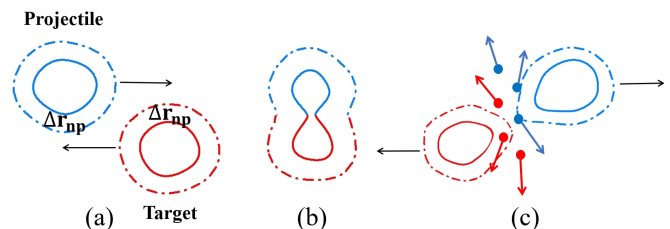


FIG. 1. Schematic diagram of peripheral heavy ion collisions. (a) initial stage, (b) reaction stage, (c) light particle emitting stage.

To quantitatively understand the neutron skin effects on heavy ion collisions observables, we simulate the collisions of $^{124,132}\text{Sn} + ^{124}\text{Sn}$ at the beam energy of 200 MeV/u and the impact parameter b ranging from $b=5$

fm to b_{max} fm with $\Delta b=0.5$ fm. b_{max} is calculated as,

$$b_{max} = R_{proj}^{max} + R_{tar}^{max} + 2.2(a_{proj}^{max} + a_{tar}^{max}). \quad (6)$$

For each impact parameter, 5000 events were simulated. The values of the half density radius $R_{proj/tar}^{max}$ are the maximum one between the neutron half density radius and the proton half density radius of projectile or target, and the values of $a_{proj/tar}^{max}$ have the similar meaning. The values of $R_{n/p}$ and $a_{n/p}$ are obtained with RDV and are listed in Table II. The term with $2.2a^{max}$ in the Eq.(6) is used for considering the surface thickness of the nucleus.

In Fig. 2 panel (a), we present the $P_{A>100}(b)$, which means the probability of observing a primary heavy residue with mass number $A > 100$ in the forward region, i.e., projectile-like residue. The red lines are the results of $^{132}\text{Sn}+^{124}\text{Sn}$, and the black lines are the results of $^{124}\text{Sn}+^{124}\text{Sn}$. The $P_{A>100}(b)$ quickly increases from zero to one from semi-peripheral to peripheral collisions, i.e., in the range of $b = 6.2 - 9.2$ fm ($b = 6.6 - 10.0$ fm), for $^{132}\text{Sn}+^{124}\text{Sn}$ ($^{124}\text{Sn}+^{124}\text{Sn}$). This behavior is determined by the reaction mechanism. When $b < 6$ fm, multifragmentation occurs and there are no fragments with $A > 100$. At $b > 10$ fm, the distance between the projectile and the target is large enough to produce the heavy projectile-like residue with $A > 100$ in each event, and then $P_{A>100}(b) = 1$. The interesting point is that curves of $P_{A>100}(b)$ show a sensitivity to the thickness of the neutron skin, or to the slope of the symmetry energy. In the range of $b = 6 - 10$ fm, the larger the values of L , the greater the $P_{A>100}$. This is because the calculations with smaller L can reach a higher density in the overlap region and more compressional energy is stored, than that for the calculations with large L . Thus, the reaction system simulated with smaller L disintegrates into more light fragments compared to the case of the calculations with large L . Owing to the conservation of the nucleon number in the reaction system, the production of projectile-like residues with $A > 100$ calculated with larger L is higher than that with smaller L . It is consistent with the calculations in Refs. [74, 75].

For understanding where the projectile-like residues can be detected, we also present the $\theta_{c.m.}$ distribution of projectile-like residues in panel (b). The projectile-like residues deflect in a small direction along the beam direction and are distributed within $\theta_{c.m.} < 4^\circ$.

The cross section for the projectile-like residues with $A > 100$ is calculated as,

$$\sigma_{A>100} = 2\pi \int_0^{b_{max}} P_{A>100}(b) b db. \quad (7)$$

In Fig. 3, the $\sigma_{A>100}$ as a function of the neutron skin thickness of system, i.e.,

$$\Delta R = \Delta r_{np}^{proj} + \Delta r_{np}^{targ}, \quad (8)$$

are presented. The panels (a) and (b) are for $^{124}\text{Sn}+^{124}\text{Sn}$ and $^{132}\text{Sn}+^{124}\text{Sn}$, respectively. The calculations illustrate that $\sigma_{A>100}$ increases with ΔR , or the slope of the symmetry energy, for both systems.

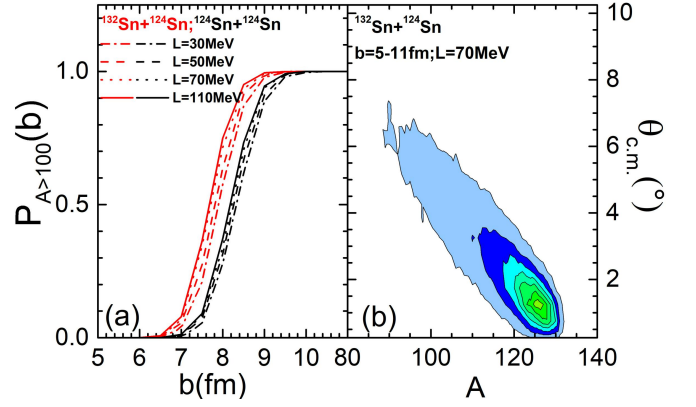


FIG. 2. (Color online) Panel (a) is the impact parameter dependence of the probability of the primary projectile-like residues with $A > 100$. Panel (b) is the $\theta_{c.m.}$ distribution of the projectile-like residues with mass number A .

For $^{124}\text{Sn}+^{124}\text{Sn}$, the $\sigma_{A>100}$ is enhanced by a factor of $\sim 5.2\%$ as ΔR increases from 0.33 fm to 0.526 fm, or as L varies from 30 to 110 MeV. For $^{132}\text{Sn}+^{124}\text{Sn}$, the $\sigma_{A>100}$ is enhanced by a factor of $\sim 5.4\%$ as ΔR increases from 0.397 fm to 0.624 fm. Thus, measuring the $\sigma_{A>100}$ could be used to obtain the neutron skin of the nucleus and the slope of the symmetry energy.

Nevertheless, the calculated results of $\sigma_{A>100}$ may be model dependent or biased. One needs to seek a way to avoid or at least suppress the possible systematic uncertainty caused by the model. Ideally, the difference of $\sigma_{A>100}$ between system A_{sys} and B_{sys} , i.e.,

$$\delta\sigma_{A>100} = \sigma_{A>100}(A_{sys}) - \sigma_{A>100}(B_{sys}), \quad (9)$$

where $A_{sys}=^{132}\text{Sn}+^{124}\text{Sn}$ and $B_{sys}=^{124}\text{Sn}+^{124}\text{Sn}$, can be used. It is based on the situation that the systematic uncertainty caused by the same model is similar for the two systems. In panel (c), we present $\delta\sigma_{A>100}$ as a function of difference of neutron skin between A_{sys} and B_{sys} , i.e.,

$$\delta R = \Delta R(A_{sys}) - \Delta R(B_{sys}). \quad (10)$$

Our calculations show that $\delta\sigma_{A>100}$ keeps the sensitivity to δR and L . So, $\delta\sigma_{A>100}$ could be used to probe the neutron skin of unstable nuclei and constrain the symmetry energy.

As charge size of fragments can be more easily measured than the mass of fragments, we also studied the sensitivity of the cross section for the projectile-like residues with the charge number $Z > 40$ to L . Our calculations show that $\sigma_{Z>40}$ is also sensitive to the L , but the sensitivity becomes weaker than $\sigma_{A>100}$. This is because the cross section measured by $\sigma_{Z>40}$ loss the information of the neutron number of fragments, so the sensitivity of $\sigma_{Z>40}$ to L is weaker than $\sigma_{A>100}$.

Then, we analyze the neutron to proton yield ratio in the transverse direction. The transverse direction in this work corresponds to $70^\circ < \theta_{c.m.} < 110^\circ$ in the center-of-mass frame. This observable was first proposed to probe

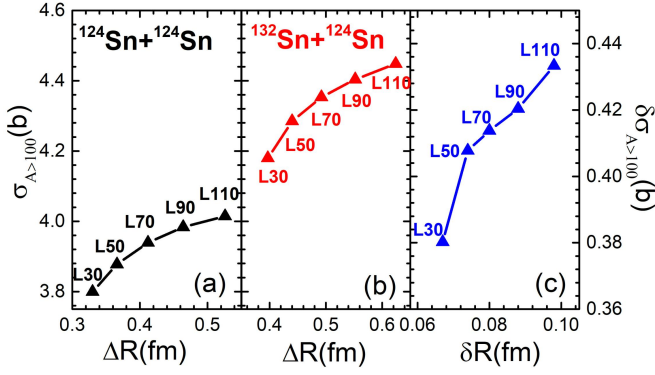


FIG. 3. (Color online) Panels (a) and (b) are the cross section of the projectile-like residues with $A > 100$ as the function of the neutron skin of the system ΔR for $^{124}\text{Sn}+^{124}\text{Sn}$ and $^{132}\text{Sn}+^{124}\text{Sn}$, respectively. Panel (c) is the $\delta\sigma_{A>100}$ as a function of δR .

the strength of the symmetry potential in Ref. [76], and has been studied extensively for constraining the symmetry energy and effective mass splitting[51, 74, 77–84].

In this work, $R(n/p)$ is obtained for peripheral collisions with the impact parameter ranging from 5 fm to 11 fm as,

$$R(n/p) = \int_{b=5}^{11} \frac{dY_n(b)}{dE_k} 2\pi b db / \int_{b=5}^{11} \frac{dY_p(b)}{dE_k} 2\pi b db. \quad (11)$$

This mainly reflects the information of the isospin contents of the overlap region, which is strongly correlated with the thickness of the neutron skin and the slope of the symmetry energy. The calculated results for $R(n/p)$ are presented in Fig. 4 (a) and (b). The black, red, and blue regions are the results for three values of ΔR , corresponding to $L=30, 70$ and 110 MeV, respectively. The panel (a) is for $^{124}\text{Sn}+^{124}\text{Sn}$, and the panel (b) is for $^{132}\text{Sn}+^{124}\text{Sn}$ system. For the emitted nucleons with kinetic energy $E_k < 80$ MeV, the $R(n/p)$ values are greater for thin neutron skin than that for thick neutron skin. It corresponds to the $R(n/p)$ values being greater for the symmetry energy with a small L case than that for the symmetry energy with a large L . The reason is that the emitted nucleons with lower kinetic energy mainly come from the subsaturation density region, where the symmetry energy obtained with small L is larger than that with large L . In addition, the stronger effects are observed for $^{132}\text{Sn}+^{124}\text{Sn}$ than for $^{124}\text{Sn}+^{124}\text{Sn}$.

For the emitted nucleons with kinetic energy $E_k \geq 80$ MeV, the $R(n/p)$ values are greater for the symmetry energy with a large L case than that for the symmetry energy with a small L . The reason is that the emitted nucleons with high kinetic energy mainly come from the high density region, where the symmetry energy obtained with large L is larger than that with small L . The calculations show that $R(n/p)$ increases with ΔR , but with large uncertainties. To further reduce the uncertainty and distinguish ΔR with a higher accuracy, the statistics

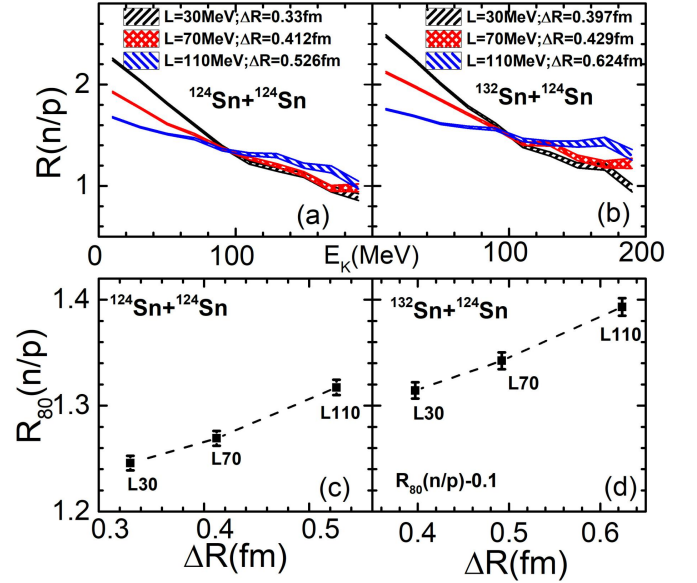


FIG. 4. (Color online) Panel (a) and (b), $R(n/p)$ as the function of the kinetic energy of the emitted nucleons, (c) and (d) are $R_{80}(n/p)$ as the function of ΔR . $R_{80}(n/p)$ is the ratio of all nucleons above 80 MeV, as shown in Eq.(12). The left panels are for $^{124}\text{Sn}+^{124}\text{Sn}$ and the right for $^{132}\text{Sn}+^{124}\text{Sn}$, respectively. To illustrate the results of two systems in a similar scale, the value of $R_{80}(n/p)$ for $^{132}\text{Sn}+^{124}\text{Sn}$ is shifted down by 0.1 in the panel(d).

in simulations must be increased. Another way is to integrate the yields of neutrons and protons above 80 MeV and then calculate the neutron to proton ratio as,

$$R_{80}(n/p) = \frac{\int_{b=5}^{11} Y_n(b, E_k \geq 80) 2\pi b db}{\int_{b=5}^{11} Y_p(b, E_k \geq 80) 2\pi b db}. \quad (12)$$

In panels (c) and (d), we present $R_{80}(n/p)$ as a function of ΔR for $^{124}\text{Sn}+^{124}\text{Sn}$ and $^{132}\text{Sn}+^{124}\text{Sn}$, respectively. According to the absolute statistical uncertainty of $R_{80}(n/p)$ in the current calculation, i.e., $err(R_{80}) = 0.01$, one can distinguish the neutron skin of the unstable nucleus with an accuracy of ~ 0.02 fm.

IV. SUMMARY AND OUTLOOK

In summary, we consistently correlate the neutron skin of nuclei in the initialization and the isospin dependent mean-field potential in nucleon propagation with the same energy density functional in the improved quantum molecular dynamics for probing the neutron skin of unstable nucleus. The unstable nucleus of ^{132}Sn on the target ^{124}Sn at peripheral collisions and the beam energy of 200 MeV per nucleon is simulated. Our calculations show that the cross section of projectile-like residues $\sigma_{A>100}$ are correlated with the neutron skin of the system. To avoid the possible systematic deviations from the model, we also construct an observable $\delta\sigma_{A>100} = \sigma_{A>100}(A_{sys}) - \sigma_{A>100}(B_{sys})$, which reflects the differ-

ence of $\sigma_{A>100}$ between two systems $A_{sys}=^{132}\text{Sn}+^{124}\text{Sn}$ and $B_{sys}=^{124}\text{Sn}+^{124}\text{Sn}$. Our calculations illustrate that $\delta\sigma_{A>100}$ keeps the sensitivity to the thickness of the neutron skin of the unstable nucleus and the slope of the symmetry energy.

In addition, the neutron to proton yield ratios, i.e., $R(n/p)$, are also sensitive to the thickness of the neutron skin. At low kinetic energy region, $R(n/p)$ is negatively correlated with the thickness of the neutron skin. At high kinetic energy region, $R(n/p)$ is positively correlated with the thickness of the neutron skin. Thus, the combination analysis on the $\delta\sigma_{A>100}$ and $R(n/p)$ at different kinetic energy regions could improve the reliability and accuracy of the measurements of neutron skin by using heavy ion collisions.

However one should note that the probe of $\delta\sigma_{A>100}$ requires experimentalists to develop a method for reconstructing primary projectile-like residues from the emitted light particles and cold fragments. Currently, a kinematical focusing method has been developed for the reconstruction of intermediate-mass fragments in Ref. [85]. Even though there will be many difficulties in recon-

structing the primary projectile-like residues, it still implies that the observables constructed from primary projectile-like residues may be in practical use in the future, and the probe of $\delta\sigma_{A>100}$ and $R(n/p)$ should be considered into the potential wish list of experimenters.

ACKNOWLEDGEMENTS

The authors thank the useful discussion with Prof. Z.G. Xiao and W.P. Lin. This work was partly inspired by the transport code comparison project, and it was supported by the National Natural Science Foundation of China Nos. 12275359, 11875323, and 11961141003, the National Key R&D Program of China under Grant No. 2018YFA0404404, the Continuous Basic Scientific Research Project (No. WDJC-2019-13, BJ20002501), and the funding of China Institute of Atomic Energy (No. YZ222407001301). The work was carried out at National Supercomputer Center in Tianjin, and the calculations were performed on TianHe-1 (A).

-
- [1] B. Alex Brown, Neutron radii in nuclei and the neutron equation of state, *Phys. Rev. Lett.* **85**, 5296 (2000).
 - [2] S. Typel and B. A. Brown, Neutron radii and the neutron equation of state in relativistic models, *Phys. Rev. C* **64**, 027302 (2001).
 - [3] R. Furnstahl, Neutron radii in mean-field models, *Nuclear Physics A* **706**, 85 (2002).
 - [4] Z. Zhang and L.-W. Chen, Constraining the symmetry energy at subsaturation densities using isotope binding energy difference and neutron skin thickness, *Physics Letters B* **726**, 234 (2013).
 - [5] C. J. Horowitz and J. Piekarewicz, Neutron star structure and the neutron radius of ^{208}Pb , *Phys. Rev. Lett.* **86**, 5647 (2001).
 - [6] X. Roca-Maza, M. Centelles, X. Viñas, and M. Warda, Neutron skin of ^{208}Pb , nuclear symmetry energy, and the parity radius experiment, *Phys. Rev. Lett.* **106**, 252501 (2011).
 - [7] G. Fricke, C. Bernhardt, K. Heilig, L. Schaller, L. Schellenberg, E. Spera, and C. Dejager, Nuclear ground state charge radii from electromagnetic interactions, *Atomic Data and Nuclear Data Tables* **60**, 177 (1995).
 - [8] I. Angeli, Y. P. Gangrsky, K. P. Marinova, I. N. Boboshin, S. Y. Komarov, B. S. Ishkhanov, and V. V. Varlamov, N and z dependence of nuclear charge radii, *Journal of Physics G: Nuclear and Particle Physics* **36**, 085102 (2009).
 - [9] I. Angeli and K. Marinova, Table of experimental nuclear ground state charge radii: An update, *Atomic Data and Nuclear Data Tables* **99**, 69 (2013).
 - [10] L. Ray, Proton-nucleus total cross sections in the intermediate energy range, *Phys. Rev. C* **20**, 1857 (1979).
 - [11] G. W. Hoffmann, L. Ray, M. Barlett, J. McGill, G. S. Adams, G. J. Igo, F. Irom, A. T. M. Wang, C. A. Whitten, R. L. Boudrie, J. F. Amann, C. Glashauser, N. M. Hintz, G. S. Kyle, and G. S. Blanpied, 0.8 gev $p+^{208}\text{Pb}$ elastic scattering and the quantity Δr_{np} , *Phys. Rev. C* **21**, 1488 (1980).
 - [12] V. E. Starodubsky and N. M. Hintz, Extraction of neutron densities from elastic proton scattering by $^{206,207,208}\text{Pb}$ at 650 mev, *Phys. Rev. C* **49**, 2118 (1994).
 - [13] Y. Kanada-En'yo, Deformation effects on the surface neutron densities of stable s and ni isotopes probed by proton elastic scattering via isotopic analysis, *arXiv*, 13 (2022).
 - [14] J. Zenihiro, H. Sakaguchi, T. Murakami, M. Yosoi, Y. Yasuda, S. Terashima, Y. Iwao, H. Takeda, M. Itoh, H. P. Yoshida, and M. Uchida, Neutron density distributions of $^{204,206,208}\text{Pb}$ deduced via proton elastic scattering at $E_p = 295$ mev, *Phys. Rev. C* **82**, 044611 (2010).
 - [15] S. Terashima, H. Sakaguchi, H. Takeda, T. Ishikawa, M. Itoh, T. Kawabata, T. Murakami, M. Uchida, Y. Yasuda, M. Yosoi, J. Zenihiro, H. P. Yoshida, T. Noro, T. Ishida, S. Asaji, and T. Yonemura, Proton elastic scattering from tin isotopes at 295 mev and systematic change of neutron density distributions, *Phys. Rev. C* **77**, 024317 (2008).
 - [16] J. Jastrzebski, A. Trzcińska, B. Klos, F. J. Hartmann, T. v. Egidy, and S. Wycech, Neutron density distributions from antiprotonic ^{208}Pb and ^{209}Bi atoms, *Phys. Rev. C* **76**, 014311 (2007).
 - [17] A. Krasznahorkay, H. Akimune, A. van den Berg, N. Blasi, S. Brandenburg, M. Csatos, M. Fujiwara, J. Gulyas, M. Harakeh, M. Hunyadi, M. de Huu, Z. Mate, D. Sohler, S. van der Werf, H. Wortche, and L. Zolnai, Neutron-skin thickness in neutron-rich isotopes, *Nuclear Physics A* **731**, 224 (2004).
 - [18] A. Krasznahorkay, A. Balanda, J. Bordewijk, S. Brandenburg, M. Harakeh, N. Kalantar-Nayestanaki, B. Nyako, J. Timar, and A. van der Woude, Excitation

- of the isovector g_{dr} by inelastic α -scattering as a measure of the neutron skin of nuclei, *Nuclear Physics A* **567**, 521 (1994).
- [19] C. M. Tarbert, D. P. Watts, D. I. Glazier, P. Aguar, J. Ahrens, J. R. M. Annand, H. J. Arends, R. Beck, V. Bekrenev, B. Boillat, A. Braghieri, D. Branford, W. J. Briscoe, J. Brudvik, S. Cherepnya, R. Codling, E. J. Downie, K. Foehl, P. Grabmayr, R. Gregor, E. Heid, D. Hornidge, O. Jahn, V. L. Kashevarov, A. Knezevic, R. Kondratiev, M. Korolija, M. Kotulla, D. Krambrich, B. Krusche, M. Lang, V. Lisin, K. Livingston, S. Lugert, I. J. D. MacGregor, D. M. Manley, M. Martinez, J. C. McGeorge, D. Mekterovic, V. Metag, B. M. K. Nefkens, A. Nikolaev, R. Novotny, R. O. Owens, P. Pedroni, A. Polonski, S. N. Prakhov, J. W. Price, G. Rosner, M. Rost, T. Rostomyan, S. Schadmand, S. Schumann, D. Sober, A. Starostin, I. Supek, A. Thomas, M. Unverzagt, T. Walcher, L. Zana, and F. Zehr (Crystal Ball at MAMI and A2 Collaboration), Neutron skin of ^{208}Pb from coherent pion photoproduction, *Phys. Rev. Lett.* **112**, 242502 (2014).
 - [20] A. Trzcińska, J. Jastrzębski, P. Lubiński, F. J. Hartmann, R. Schmidt, T. von Egidy, and B. Klos, Neutron density distributions deduced from antiprotonic atoms, *Phys. Rev. Lett.* **87**, 082501 (2001).
 - [21] J. Jastrzębski, A. Trzcinska, P. Lubinski, B. Klos, F. J. Hartmann, T. von Egidy, and S. Wycech, Neutron density distributions from antiprotonic atoms compared with hadron scattering data, *International Journal of Modern Physics E* **13**, 343 (2004).
 - [22] B. A. Brown, G. Shen, G. C. Hillhouse, J. Meng, and A. Trzcinska, Neutron skin deduced from antiprotonic atom data, *Phys. Rev. C* **76**, 034305 (2007).
 - [23] HaojieXu, Constraints on neutron skin thickness and nuclear deformations using relativistic heavy-ion collisions from star*, arXiv **2208**, 06149v1 (2022).
 - [24] L.-M. Liu, J. Xu, and G.-X. Peng, Measuring deformed neutron skin with free spectator nucleons in relativistic heavy-ion collisions, *Physics Letters B* **838**, 137701 (2023).
 - [25] HaojieXu, H. Li, X. Wang, C. Shen, and F. Wang, Determine the neutron skin type by relativistic isobaric collisions, *Physics Letters B* **819**, 136453 (2021).
 - [26] H. Li, HaojieXu, Y. Zhou, X. Wang, J. Zhao, L.-W. Chen, and F. Wang, Probing the neutron skin with ultrarelativistic isobaric collisions, *Phys. Rev. Lett.* **125**, 222301 (2020).
 - [27] C. J. Horowitz, S. J. Pollock, P. A. Souder, and R. Michaels, Parity violating measurements of neutron densities, *Phys. Rev. C* **63**, 025501 (2001).
 - [28] C. J. Horowitz, Z. Ahmed, C.-M. Jen, A. Rakhman, P. A. Souder, M. M. Dalton, N. Liyanage, K. D. Paschke, K. Saenboonruang, R. Silwal, G. B. Franklin, M. Friend, B. Quinn, K. S. Kumar, D. McNulty, L. Mercado, S. Riordan, J. Wexler, R. W. Michaels, and G. M. Urciuoli, Weak charge form factor and radius of ^{208}Pb through parity violation in electron scattering, *Phys. Rev. C* **85**, 032501 (2012).
 - [29] S. Abrahamyan, Z. Ahmed, H. Albataineh, K. Aniol, D. S. Armstrong, W. Armstrong, T. Averett, B. Babineau, A. Barbieri, V. Bellini, R. Beminiwattha, J. Benesch, F. Benmokhtar, T. Bielarski, W. Boeglin, A. Camsonne, M. Canan, P. Carter, G. D. Cates, C. Chen, J.-P. Chen, O. Hen, F. Cusanno, M. M. Dalton, R. De Leo, K. de Jager, W. Deconinck, P. Decowski, X. Deng, A. Deur, D. Dutta, A. Etile, D. Flay, G. B. Franklin, M. Friend, S. Frullani, E. Fuchey, F. Garibaldi, E. Gasser, R. Gilman, A. Giusa, A. Glamazdin, J. Gomez, J. Grames, C. Gu, O. Hansen, J. Hansknecht, D. W. Higinbotham, R. S. Holmes, T. Holmstrom, C. J. Horowitz, J. Hoskins, J. Huang, C. E. Hyde, F. Itard, C.-M. Jen, E. Jensen, G. Jin, S. Johnston, A. Kelleher, K. Kliakhandler, P. M. King, S. Kowalski, K. S. Kumar, J. Leacock, J. Leckey, J. H. Lee, J. J. LeRose, R. Lindgren, N. Liyanage, N. Lubinsky, J. Mammei, F. Mammoliti, D. J. Margaziotis, P. Markowitz, A. McCreary, D. McNulty, L. Mercado, Z.-E. Meziani, R. W. Michaels, M. Mihovilovic, N. Muangma, C. Muñoz Camacho, S. Nanda, V. Nelyubin, N. Nuruzzaman, Y. Oh, A. Palmer, D. Parno, K. D. Paschke, S. K. Phillips, B. Poelker, R. Pomatsalyuk, M. Posik, A. J. R. Puckett, B. Quinn, A. Rakhman, P. E. Reimer, S. Riordan, P. Rogan, G. Ron, G. Russo, K. Saenboonruang, A. Saha, B. Sawatzky, A. Shahinyan, R. Silwal, S. Sirca, K. Slifer, P. Solvignon, P. A. Souder, M. L. Sperduto, R. Subedi, R. Suleiman, V. Sulkosky, C. M. Suter, W. A. Tobias, W. Troth, G. M. Urciuoli, B. Waidyawansa, D. Wang, J. Wexler, R. Wilson, B. Wojtsekhowski, X. Yan, H. Yao, Y. Ye, Z. Ye, V. Yim, L. Zana, X. Zhan, J. Zhang, Y. Zhang, X. Zheng, and P. Zhu (PREX Collaboration), Measurement of the neutron radius of ^{208}Pb through parity violation in electron scattering, *Phys. Rev. Lett.* **108**, 112502 (2012).
 - [30] D. Adhikari, H. Albataineh, D. Androic, K. Aniol, D. S. Armstrong, T. Averett, C. Ayerbe Gayoso, S. Barcus, V. Bellini, R. S. Beminiwattha, J. F. Benesch, H. Bhatt, D. Bhatta Pathak, D. Bhetuwal, B. Blaikie, Q. Campagna, A. Camsonne, G. D. Cates, Y. Chen, C. Clarke, J. C. Cornejo, S. Covrig Dusa, P. Datta, A. Deshpande, D. Dutta, C. Feldman, E. Fuchey, C. Gal, D. Gaskell, T. Gautam, M. Gericke, C. Ghosh, I. Halilovic, J.-O. Hansen, F. Hauenstein, W. Henry, C. J. Horowitz, C. Jantzi, S. Jian, S. Johnston, D. C. Jones, B. Karki, S. Katugampola, C. Keppel, P. M. King, D. E. King, M. Knauss, K. S. Kumar, T. Kutz, N. Lashley-Colthirst, G. Leverick, H. Liu, N. Liyanage, S. Malace, R. Mammei, J. Mammei, M. McCaughan, D. McNulty, D. Meekins, C. Metts, R. Michaels, M. M. Mondal, J. Napolitano, A. Narayan, D. Nikolaev, M. N. H. Rashad, V. Owen, C. Palatchi, J. Pan, B. Pandey, S. Park, K. D. Paschke, M. Petrusky, M. L. Pitt, S. Premathilake, A. J. R. Puckett, B. Quinn, R. Radloff, S. Rahman, A. Rathnayake, B. T. Reed, P. E. Reimer, R. Richards, S. Riordan, Y. Roblin, S. Seeds, A. Shahinyan, P. Souder, L. Tang, M. Thiel, Y. Tian, G. M. Urciuoli, E. W. Wertz, B. Wojtsekhowski, B. Yale, T. Ye, A. Yoon, A. Zec, W. Zhang, J. Zhang, and X. Zheng (PREX Collaboration), Accurate determination of the neutron skin thickness of ^{208}Pb through parity-violation in electron scattering, *Phys. Rev. Lett.* **126**, 172502 (2021).
 - [31] D. Adhikari, H. Albataineh, D. Androic, K. A. Aniol, D. S. Armstrong, T. Averett, C. Ayerbe Gayoso, S. K. Barcus, V. Bellini, R. S. Beminiwattha, J. F. Benesch, H. Bhatt, D. Bhatta Pathak, D. Bhetuwal, B. Blaikie, J. Boyd, Q. Campagna, A. Camsonne, G. D. Cates, Y. Chen, C. Clarke, J. C. Cornejo, S. Covrig Dusa, M. M. Dalton, P. Datta, A. Deshpande, D. Dutta, C. Feldman, E. Fuchey, C. Gal, D. Gaskell, T. Gau-

- tam, M. Gericke, C. Ghosh, I. Halilovic, J.-O. Hansen, O. Hassan, F. Hauenstein, W. Henry, C. J. Horowitz, C. Jantzi, S. Jian, S. Johnston, D. C. Jones, S. Kakkar, S. Katugampola, C. Keppel, P. M. King, D. E. King, K. S. Kumar, T. Kutz, N. Lashley-Colthirst, G. Leverick, H. Liu, N. Liyanage, J. Mammey, R. Mammey, M. McCaughan, D. McNulty, D. Meekins, C. Metts, R. Michaels, M. Mihovilovic, M. M. Mondal, J. Napolitano, A. Narayan, D. Nikolaev, V. Owen, C. Palatchi, J. Pan, B. Pandey, S. Park, K. D. Paschke, M. Petrusky, M. L. Pitt, S. Premathilake, B. Quinn, R. Radloff, S. Rahman, M. N. H. Rashad, A. Rathnayake, B. T. Reed, P. E. Reimer, R. Richards, S. Riordan, Y. R. Roblin, S. Seeds, A. Shahinyan, P. Souder, M. Thiel, Y. Tian, G. M. Urciuoli, E. W. Wertz, B. Wojtsekhowski, B. Yale, T. Ye, A. Yoon, W. Xiong, A. Zec, W. Zhang, J. Zhang, and X. Zheng (CREX Collaboration), Precision determination of the neutral weak form factor of ^{48}Ca , *Phys. Rev. Lett.* **129**, 042501 (2022).
- [32] D. Akimov, J. Albert, P. An, C. Awe, P. Barbean, B. Becker, V. Belov, A. Brown, A. Bolozydynya, B. Cabrera-Palmer, M. Cervantes, J. I. Collar, R. J. Cooper, R. L. Cooper, C. Cuesta, D. J. Dean, J. A. Detwiler, A. Eberhardt, Y. Efremenko, S. R. Elliott, and E. M. E. et al. COHERENT Collaboration, Observation of coherent elastic neutrino-nucleus scattering, *Science* **357**, 1123 (2017).
- [33] M. Cadeddu, C. Giunti, Y. F. Li, and Y. Y. Zhang, Average cs neutron density distribution from coherent data, *Phys. Rev. Lett.* **120**, 072501 (2018).
- [34] M. Centelles, X. Roca-Maza, X. Viñas, and M. Warda, Nuclear symmetry energy probed by neutron skin thickness of nuclei, *Phys. Rev. Lett.* **102**, 122502 (2009).
- [35] L.-W. Chen, C. M. Ko, B.-A. Li, and J. Xu, Density slope of the nuclear symmetry energy from the neutron skin thickness of heavy nuclei, *Phys. Rev. C* **82**, 024321 (2010).
- [36] J. Xu, W.-J. Xie, and B.-A. Li, Bayesian inference of nuclear symmetry energy from measured and imagined neutron skin thickness in $^{116,118,120,122,124,130,132}\text{Sn}$, ^{208}Pb , and ^{48}Ca , *Phys. Rev. C* **102**, 044316 (2020).
- [37] Z. Zhang and L.-W. Chen, Constraining the density slope of nuclear symmetry energy at subsaturation densities using electric dipole polarizability in ^{208}Pb , *Phys. Rev. C* **90**, 064317 (2014).
- [38] M. Oertel, M. Hempel, T. Klähn, and S. Typel, Equations of state for supernovae and compact stars, *Rev. Mod. Phys.* **89**, 015007 (2017).
- [39] B.-A. Li and X. Han, Constraining the neutron-proton effective mass splitting using empirical constraints on the density dependence of nuclear symmetry energy around normal density, *Physics Letters B* **727**, 276 (2013).
- [40] M. K. Gaidarov, A. N. Antonov, P. Sarriguren, and E. M. de Guerra, Symmetry energy of deformed neutron-rich nuclei, *Phys. Rev. C* **85**, 064319 (2012).
- [41] M. B. Tsang, J. R. Stone, F. Camera, P. Danielewicz, S. Gandolfi, K. Hebeler, C. J. Horowitz, J. Lee, W. G. Lynch, Z. Kohley, R. Lemmon, P. Möller, T. Murakami, S. Riordan, X. Roca-Maza, F. Sammarruca, A. W. Steiner, I. Vidaña, and S. J. Yennello, Constraints on the symmetry energy and neutron skins from experiments and theory, *Phys. Rev. C* **86**, 015803 (2012).
- [42] X. Viñas, M. Centelles, X. Roca-Maza, and M. Warda, Density dependence of the symmetry energy from neutron skin thickness in finite nuclei, *The European Physical Journal A* **50** (2014).
- [43] Y. Zhang, M. Liu, C.-J. Xia, Z. Li, and S. K. Biswal, Constraints on the symmetry energy and its associated parameters from nuclei to neutron stars, *Phys. Rev. C* **101**, 034303 (2020).
- [44] J. Estee, W. G. Lynch, C. Y. Tsang, J. Barney, G. Jhang, M. B. Tsang, R. Wang, M. Kaneko, J. W. Lee, T. Isobe, M. Kurata-Nishimura, T. Murakami, D. S. Ahn, L. Atar, T. Aumann, H. Baba, K. Boretzky, J. Brzychczyk, G. Cerizza, N. Chiga, N. Fukuda, I. Gasparic, B. Hong, A. Horvat, K. Ieki, N. Inabe, Y. J. Kim, T. Kobayashi, Y. Kondo, P. Lasko, H. S. Lee, Y. Leifels, J. Lukasik, J. Manfredi, A. B. McIntosh, P. Morfouace, T. Nakamura, N. Nakatsuka, S. Nishimura, H. Otsu, P. Pawlowski, K. Pelczar, D. Rossi, H. Sakurai, C. Santamaria, H. Sato, H. Scheit, R. Shane, Y. Shimizu, H. Simon, A. Snoch, A. Sochocka, T. Sumikama, H. Suzuki, D. Suzuki, H. Takeda, S. Tangwanchaoen, H. Toernqvist, Y. Togano, Z. G. Xiao, S. J. Yennello, Y. Zhang, and M. D. Cozma (S π RIT Collaboration), Probing the symmetry energy with the spectral pion ratio, *Phys. Rev. Lett.* **126**, 162701 (2021).
- [45] B.-A. Li, B.-J. Cai, W.-J. Xie, and N.-B. Zhang, Progress in constraining nuclear symmetry energy using neutron star observables since gw170817, *Universe* **7**, 10.3390/universe7060182 (2021).
- [46] R. Essick, I. Tews, P. Landry, and A. Schwenk, Astrophysical constraints on the symmetry energy and the neutron skin of ^{208}Pb with minimal modeling assumptions, *Phys. Rev. Lett.* **127**, 192701 (2021).
- [47] P. Danielewicz, P. Singh, and J. Lee, Symmetry energy iii: Isovector skins, *Nuclear Physics A* **958**, 147 (2017).
- [48] J. M. Lattimer and A. W. Steiner, Constraints on the symmetry energy using the mass-radius relation of neutron stars, *Eur. Phys. J. A* **50**, 10.1140/epja/i2014-14040-y (2014).
- [49] X. Roca-Maza, M. Brenna, G. Colò, M. Centelles, X. Viñas, B. K. Agrawal, N. Paar, D. Vretenar, and J. Piekarewicz, Electric dipole polarizability in ^{208}pb : Insights from the droplet model, *Phys. Rev. C* **88**, 024316 (2013).
- [50] J. M. Lattimer and Y. Lim, Constraining the symmetry parameters of the nuclear interaction, *The Astrophysical Journal* **771** (2013).
- [51] M. B. Tsang, Y. Zhang, P. Danielewicz, M. Famiano, Z. Li, W. G. Lynch, and A. W. Steiner, Constraints on the density dependence of the symmetry energy, *Phys. Rev. Lett.* **102**, 122701 (2009).
- [52] L. Trippa, G. Colò, and E. Vigezzi, Giant dipole resonance as a quantitative constraint on the symmetry energy, *Phys. Rev. C* **77**, 061304 (2008).
- [53] A. Tamii, I. Poltoratska, P. von Neumann-Cosel, Y. Fujita, T. Adachi, C. A. Bertulani, J. Carter, M. Dozono, H. Fujita, K. Fujita, K. Hatanaka, D. Ishikawa, M. Itoh, T. Kawabata, Y. Kalmykov, A. M. Krumbholz, E. Litvinova, H. Matsubara, K. Nakanishi, R. Neveling, H. Okamura, H. J. Ong, B. Özel-Tashenov, V. Y. Ponomarev, A. Richter, B. Rubio, H. Sakaguchi, Y. Sakemi, Y. Sasamoto, Y. Shimbara, Y. Shimizu, F. D. Smit, T. Suzuki, Y. Tameshige, J. Wambach, R. Yamada, M. Yosoi, and J. Zenihiro, Complete electric dipole response and the neutron skin in ^{208}Pb , *Phys. Rev. Lett.* **107**, 062502 (2011).

- [54] M. Kortelainen, T. Lesinski, J. Moré, W. Nazarewicz, J. Sarich, N. Schunck, M. V. Stoitsov, and S. Wild, Nuclear energy density optimization, *Phys. Rev. C* **82**, 024313 (2010).
- [55] N. Wang, L. Ou, and M. Liu, Nuclear symmetry energy from the fermi-energy difference in nuclei, *Phys. Rev. C* **87**, 034327 (2013).
- [56] B. A. Brown, Constraints on the skyrme equations of state from properties of doubly magic nuclei, *Phys. Rev. Lett.* **111**, 232502 (2013).
- [57] Z. Zhang, and L.-W. Chen, Bayesian inference of the symmetry energy and the neutron skin in ^{48}Ca and ^{208}Pb from crex and prex-2, *arXiv* **2207**, 03328v1 (2022).
- [58] B. T. Reed, F. J. Fattoyev, C. J. Horowitz, and J. Piekarewicz, Implications of prex-2 on the equation of state of neutron-rich matter, *Phys. Rev. Lett.* **126**, 172503 (2021).
- [59] S. Typel, Neutron skin thickness of heavy nuclei with α -particle correlations and the slope of the nuclear symmetry energy, *Phys. Rev. C* **89**, 064321 (2014).
- [60] J. Tanaka, Z. Yang, S. Typel, S. Adachi, S. Bai, P. van Beek, D. Beaumel, Y. Fujikawa, J. Han, S. H. S. Huang, A. Inoue, Y. Jiang, M. Knösel, N. Kobayashi, Y. Kubota, W. Liu, J. Lou, Y. Maeda, Y. Matsuda, K. Miki, S. Nakamura, K. Ogata, V. Panin, H. Scheit, F. Schindler, P. Schrock, D. Symochko, A. Tamii, T. Uesaka, V. Wagner, K. Yoshida, J. Zenihiro, and T. Aumann, Formation of α clusters in dilute neutron-rich matter, *Science* **371**, 5 (2021).
- [61] W. Horiuchi, Y. Suzuki, and T. Inakura, Probing neutron-skin thickness with total reaction cross sections, *Phys. Rev. C* **89**, 011601 (2014).
- [62] A. Krasznahorkay, M. Fujiwara, P. van Aarle, H. Akimune, I. Daito, H. Fujimura, Y. Fujita, M. N. Harakeh, T. Inomata, J. Jänecke, S. Nakayama, A. Tamii, M. Tanaka, H. Toyokawa, W. Uijen, and M. Yosoi, Excitation of isovector spin-dipole resonances and neutron skin of nuclei, *Phys. Rev. Lett.* **82**, 3216 (1999).
- [63] A. Klimkiewicz, N. Paar, P. Adrich, M. Fallot, K. Boretzky, T. Aumann, D. Cortina-Gil, U. D. Pramanik, T. W. Elze, H. Emling, H. Geissel, M. Hellström, K. L. Jones, J. V. Kratz, R. Kulessa, C. Nociforo, R. Palit, H. Simon, G. Surówka, K. Sümmerer, and D. Vretenar (LAND Collaboration), Nuclear symmetry energy and neutron skins derived from pygmy dipole resonances, *Phys. Rev. C* **76**, 051603 (2007).
- [64] T. Aumann, C. A. Bertulani, F. Schindler, and S. Typel, Peeling off neutron skins from neutron-rich nuclei: Constraints on the symmetry energy from neutron-removal cross sections, *Phys. Rev. Lett.* **119**, 262501 (2017).
- [65] C. Hartnack, A. L. Fevre, Y. Leifels, and J. Aichelin, The influence of the neutron skin and the asymmetry energy on the π^-/π^+ ratio, *arXiv* **1808**, 09868v1 (2018).
- [66] G.-F. Wei, B.-A. Li, J. Xu, and L.-W. Chen, Influence of neutron-skin thickness on the π^-/π^+ ratio in pb + pb collisions, *Phys. Rev. C* **90**, 014610 (2014).
- [67] C.-W. Ma, H.-L. Wei, X.-Q. Liu, J. Su, H. Zheng, W.-P. Lin, and Y.-X. Zhang, Nuclear fragments in projectile fragmentation reactions, *Progress in Particle and Nuclear Physics* **121**, 103911 (2021).
- [68] J. Yang, Y. Zhang, N. Wang, and Z. Li, Influence of the treatment of initialization and mean-field potential on the neutron to proton yield ratios, *Phys. Rev. C* **104**, 024605 (2021).
- [69] Y. Zhang, N. Wang, Q.-F. Li, L. Ou, J.-L. Tian, M. Liu, K. Zhao, X.-Z. Wu, and Z.-X. Li, Progress of quantum molecular dynamics model and its applications in heavy ion collisions, *Front. Phys.* **15**, 54301 (2020).
- [70] T.H.R.Skyrme, The nuclear surface, *Philos. Mag* **1**, 1043 (1956).
- [71] Y. Zhang and Z. Li, Elliptic flow and system size dependence of transition energies at intermediate energies, *Phys. Rev. C* **74**, 014602 (2006).
- [72] L. Min, W. Ning, L. Zhu-Xia, and W. Xi-Zhen, Neutron skin thickness of nuclei and effective nucleon-nucleon interactions, *Chinese Physics Letters* **23**, 804 (2006).
- [73] M. Brack, C. Guet, and H.-B. Hakansson, Selfconsistent semiclassical description of average nuclear properties a link between microscopic and macroscopic models, *Physics Reports* **123**, 275 (1985).
- [74] Y. Zhang, D. D. S. Coupland, P. Danielewicz, Z. Li, H. Liu, F. Lu, W. G. Lynch, and M. B. Tsang, Influence of in-medium nn cross sections, symmetry potential, and impact parameter on isospin observables, *Phys. Rev. C* **85**, 024602 (2012).
- [75] L. Li, F. Wang, and Y. Zhang, Isospin effects on intermediate mass fragments at intermediate energy-heavy ion collisions, *Nuclear Science and Techniques* **33**, 58 (2022).
- [76] B.-A. Li, C. M. Ko, and Z. Ren, Equation of state of asymmetric nuclear matter and collisions of neutron-rich nuclei, *Phys. Rev. Lett.* **78**, 1644 (1997).
- [77] Y. Zhang, P. Danielewicz, M. Famiano, Z. Li, W. Lynch, and M. Tsang, The influence of cluster emission and the symmetry energy on neutron-proton spectral double ratios, *Physics Letters B* **664**, 145 (2008).
- [78] J. Su, L. Zhu, C.-Y. Huang, W.-J. Xie, and F.-S. Zhang, Correlation between symmetry energy and effective k -mass splitting with an improved isospin- and momentum-dependent interaction, *Phys. Rev. C* **94**, 034619 (2016).
- [79] Z.-Q. Feng, Transverse emission of isospin ratios as a probe of high-density symmetry energy in isotopic nuclear reactions, *Physics Letters B* **707**, 83 (2012).
- [80] A. Ono, P. Danielewicz, W. A. Friedman, W. G. Lynch, and M. B. Tsang, Isospin fractionation and isoscaling in dynamical simulations of nuclear collisions, *Phys. Rev. C* **68**, 051601 (2003).
- [81] B.-A. Li, L.-W. Chen, G.-C. Yong, and W. Zuo, Double neutron/proton ratio of nucleon emissions in isotopic reaction systems as a robust probe of nuclear symmetry energy, *Physics Letters B* **634**, 378 (2006).
- [82] Q. Li, Z. Li, and H. Stöcker, Probing the symmetry energy and the degree of isospin equilibrium, *Phys. Rev. C* **73**, 051601 (2006).
- [83] Y. Zhang, M. Tsang, Z. Li, and H. Liu, Constraints on nucleon effective mass splitting with heavy ion collisions, *Physics Letters B* **732**, 186 (2014).
- [84] D. D. S. Coupland, M. Youngs, Z. Chajecki, W. G. Lynch, M. B. Tsang, Y. X. Zhang, M. A. Famiano, T. K. Ghosh, B. Giacherio, M. A. Kilburn, J. Lee, H. Liu, F. Lu, P. Morfouace, P. Russotto, A. Sanetullaev, R. H. Showalter, G. Verde, and J. Winkelbauer, Probing effective nucleon masses with heavy-ion collisions, *Phys. Rev. C* **94**, 011601 (2016).
- [85] W. Lin, X. Liu, M. R. D. Rodrigues, S. Kowalski, R. Wada, M. Huang, S. Zhang, Z. Chen, J. Wang, G. Q. Xiao, R. Han, Z. Jin, J. Liu, P. Ren, F. Shi, T. Keutgen, K. Hagel, M. Barbui, C. Bottosso, A. Bonasera,

J. B. Natowitz, T. Materna, L. Qin, P. K. Sahu, and H. Zheng, Experimental reconstruction of primary hot isotopes and characteristic properties of the fragmenting

source in heavy-ion reactions near the fermi energy, Phys. Rev. C **90**, 044603 (2014).